J Mol Model (2012) 18:3751–3768
DOI 10.1007/s00894-012-1356-9

ORIGINAL PAPER

Odd-electron molecular theory of graphene hydrogenation

Elena F. Sheka · Nadezhda A. Popova

Received: 20 October 2011 / Accepted: 5 January 2012 / Published online: 7 March 2012

Abstract This paper highlights the molecular essence of graphene and presents its hydrogenation from the viewpoint of the odd-electron molecular theory. This chemical transformation was performed computationally, using a particular algorithm, through the stepwise addition of either hydrogen molecules or hydrogen atoms to a pristine graphene molecule. The graphene was considered to be a membrane, such that either both sides or just one side of the membrane was accessible to adsorbate, and the atoms on the perimeter of the membrane were either fixed (fixed membrane) or free to move (free-standing membrane). The algorithm explored the spatial distribution of the number of effectively unpaired electrons N_{DA} over the carbon skeleton of the molecule. The highest ranked N_{DA} values were considered to indicate the target atoms at each reaction step. The dependence of the hydrogenation itself and the final graphene hydrides on external factors such as whether the membrane was fixed, if both sides or only one side of the membrane were accessible to hydrogen, and whether the hydrogen was in the molecular or atomic state. Complete hydrogenation followed by the formation of a regular chair-like graphane structure $(CH)_n$ was only found to be possible for a fixed pristine graphene membrane for which the basal plane is accessible to hydrogen atoms from both sides.

Keywords Hydrogenation · Graphene · Graphane · Cyclohexane · Isomers · Quantum chemistry · Unrestricted broken symmetry approach · Atom chemical susceptibility

E. F. Sheka (✉) · N. A. Popova
Peoples' Friendship University of Russia,
Miklukho-Maklaya 6,
Moscow 117198, Russia
e-mail: sheka@icp.ac.ru

Introduction

The report "Control of graphene's properties by reversible hydrogenation: evidence for graphane" [1], published in *Science* in January 2009, presented the discovery of a new two-dimensional crystalline material termed *graphane*. The material was obtained in due course of the adsorption of atomic hydrogen onto graphene. TEM analysis has shown that the new material demonstrates crystalline properties that are characteristic of hexagonal crystals. In contrast with graphene, which is characterized by high conductivity, graphane is dielectric. Therefore, for the first time, it has been demonstrated that graphene can be transformed into another material characterized by very different properties following chemical modification. In practice, this discovery has led to new hope that pristine graphene can be tailored into materials with specific conductive properties by "fine tuning" via chemical modification. The importance of graphane as heralding the possibility of such transformations has led some to declare that "graphane—the son of graphene—is the grandfather of electronics of the future" [2].

The significance of this discovery can be inferred from the fact that, among the ~2000 publications devoted to graphene in 2010 [2, 3], a few tens of them [4–31] are related to graphane either directly or indirectly (i.e., they just mention it). This publication list is quite peculiar, as only one of the papers is an experimental study [5], while the others relate to different theoretical and/or computational aspects of the graphane science. This finding clearly highlights that—in spite of the fact that hydrogen-modified single layers of graphite have been discussed for some time now (see [32] and references therein), and these discussions have moved from focusing on the theoretical and

computational aspects of this subject to more practical aspects since 2009 [1], which has resulted in a drastic growth of interest in research in multiple fields relating to this topic—there are still many unresolved problems that need to be highlighted and solved.

To facilitate the consideration of the problems as well as suggested approaches to solving them, let us conditionally select three aspects, namely: theoretical, computational, and molecular around which are concentrated two-dimensional crystal theory, computational approaches and/or algorithms, and molecular quantum theory.

Theoretical studies mainly focus on solid-state aspects of graphane (see the exhaustive review [31] on graphene from a theoretical perspective), particularly those relating to the influence of the chemical modification of pristine graphene on specific properties of the two-dimensional graphene crystal. If we only consider work done on hydrogenation, bandgap opening induced by patterned hydrogen adsorption [6], magnetic properties of graphene–graphane superlattices [7, 8], high-temperature electron–phonon superconductivity [9, 10], Bose–Einstein condensation of excitons [11], giant Faraday rotation [12], the possible creation of quantum dots as vacancy clusters in the body of graphane [13], and the nanomechanics of hydrogenated graphene [14–17] are the topics of the studies that have been performed so far.

The vast majority of the studies that have adopted a computational approach to this subject [5–32] have made use of DFT computational schemes, although a few studies have been performed using molecular dynamics [17–19]. DFT schemes with different configurations have been applied, but they do have a common characteristic: the calculations, with only one exception [23], have been performed using a closed-shell approach (a restricted computational scheme in other words) that does not take into account the spin correlation of odd electrons in pristine graphene playing an influential role in the behavior of its electronic system [33–37]. The spin correlation means that effectively unpaired electrons must be accounted for during incomplete graphene hydrogenation and when considering vacancies inside graphane consisting of graphene clusters.

The abovementioned DFT studies focus mainly on the solid-state aspects of the graphane crystal, which is why they are based on a supercell with periodic boundary conditions (PBC). In most cases, the supercell is just the unit cell of the chairlike conformer of the graphane crystal. The unit cells of more complicated structures, determined quite arbitrarily beforehand, are also exploited in studies devoted to elucidating the peculiarities of the electronic system of graphane itself, as well as its physicochemical properties [17, 20–24].

In contrast, the odd-electron molecular theory of graphene focuses mainly on the peculiarities of its sp^2-hybridized electron system, which facilitates the extensive use of quantum chemistry when studying molecules. It has been recently shown by the authors that odd-electron theory is very effective when applied to basic graphene problems, such as when studying the formation of particular composites between carbon nanotubes and graphene [38] or fullerene C_{60} and graphene [39], or when considering the tensile deformation and fracture of nanosized graphene [40, 41] and graphane [42] molecules during a mechanochemical reaction. The optimistic results obtained in the studies make it possible to shift attention from problems relating solid-state graphane so that the following questions can be considered: what is the reaction for graphene hydrogenation; what are the final products of this reaction; and under which conditions can we expect these products to be formed? In the current paper, we present the results of our study in which we attempted to answer the preceding three questions using odd-electron theory.

Algorithmic computational generation of graphene polyhydrides $(CH)_n$

From a chemical perspective, the hydrogenation of graphene results from the adsorption of hydrogen onto the basal plane of either graphite or graphene. Both of these structural configurations are practically equivalent from a computational viewpoint due to the relatively weak interactions between neighboring graphite layers. Thus, computational studies of the adsorption of hydrogen onto graphite consider one or two layers of substrate [32, 43–46]. This is why the hydrogenation of graphene was studied long before the material was actually obtained experimentally. These studies have shown that the following issues must be addressed when designing the computational problem:

1. Is the hydrogen more likely to be adsorbed as molecules or atoms?
2. What is the characteristic image of the attachment of a hydrogen atom to the substrate?
3. Which carbon atom is the first target for hydrogen attachment?
4. How carbon atoms of the substrate are selected for the subsequent steps of the adsorption?
5. Is there any connection between the hexagonal pattern of the sequential adsorption and cyclohexane conformers?

It is known experimentally that the molecular adsorption of hydrogen onto graphite is extremely weak, so its hydrogenation only occurs in a plasma containing atomic hydrogen. As far as we are aware, molecular adsorption of hydrogen by graphite has not yet been considered computationally.

In the first paper in which the adsorption of a single hydrogen atom onto a graphite substrate was explored via DFT [43], it was shown that the hydrogen was accommodated

at the top carbon atom, forming a characteristic C–H bond 1.11 Å in length, and this caused significant deformation of the substrate due to the transformation of the sp^2 configuration of this carbon atom before hydrogenation into the sp^3 configuration after adsorption. Both issues are highly characteristic for individual adsorption event and significantly influence the formation of final product.

The specific sites at which the adsorption events occurred on the graphite substrate were studied in the framework of classical supercell–PBC DFT using restricted (RDFT) [32] and unrestricted (UDFT) [44] computational schemes. Sites for the first adsorption were chosen arbitrarily, while sites for the subsequent hydrogen depositions were chosen according to the lowest-energy criterion. While only two hydrogen atoms were added in [44], eight atoms were adsorbed in a $3\times3\times1$ supercell in [32], and 46 individual sites were considered in that work. It is worth noting that the latter study should be related to the first study on graphene, since the substrate was arranged as a single graphite layer. At the same time, the authors of the latter study restricted themselves to adsorption on only one side of the layer, due to the inaccessibility of its other side to hydrogen gas in the bulk graphite. Addressing graphene, the authors of [46] performed classical molecular dynamics calculations on graphene, studying the accommodation of an individual hydrogen atom or a pair of them onto clusters consisting of 50 or 160 carbon atoms, respectively. They obtained results that were quite similar to those obtained for graphite [43]. A similar approach to graphene sheet hydrogenation was also used in some recent papers [47, 48] based on spin-polarized DFT calculations. The best deposition site was again chosen according to the lowest-energy criterion. These studies showed that the adsorption of hydrogen onto either the graphite or graphene basal plane is possible, but the final product does not represent a new material; it is simply a chemically modified graphite and/or graphene patterned with hydrogen adsorbates.

The first time the formation of a new material due to the chemical modification of graphite was considered in a study focusing on the formation of graphite polyfluoride $(CF)_n$ (for a comprehensive review, see [49]). For that study, Charlier et al. suggested a well-defined, regular, chairlike structure that was supported computationally [50]. $(CH)_n$ and $(CF)_n$ species are referred to in the literature as monohydride and monofluoride graphene, respectively. This notation is attributed to crystals with unit cells containing either CH or CF units. In a molecular approach, it would be better to consider the configurations $(CH)_n$ and $(CF)_n$ as polyderivatives of a pristine graphene molecule, as this makes it possible to consider their formation as a stepwise hydrogenation and/or fluorination.

The authors [50] followed the suggestion of Rüdorff to present the structure of the fluoride as an infinite array of *trans*-linked perfluorocyclohexane chairs [49]. The structure proposed by Rüdorff is based on the existence of two stable conformers of cyclohexane, known as the chairlike and boatlike configurations. The former conformer is more energetically favorable, but commercial products always contain a mixture of the two. Actually, there is evidence that the structure of $(CF)_n$ consists of an infinite array of *cis-trans*-linked cyclohexane boats [51], so Charlier et al. included both conformations and showed that the chairlike one is preferred.

In view of the intensified study of the graphite hydrogenation and a large resonance caused by a massive examination of both fluorinated and hydrogenated polyderivatives of fullerene C_{60}, which exhibited a deep parallelism between these two sp^2- carboneous families and achieved its maximum by 2004 [52, 53], the appearance of the paper of Sofo et al. [54] was no surprise. The authors led the parallelism of fluorinated and hydrogenated sp^2 fullerenes, whilst not referring to these fundamental studies, in the foundation of their approach and followed the same scheme of the construction and computational treatment of graphene polyhydride $(CH)_n$ that was applied by Charlier et al. [50] to polyfluorides $(CF)_n$. Thus introduced new substance was termed graphane. Just like $(CF)_n$, the chairlike conformer $(CH)_n$ appeared to be the most energetically stable, as later confirmed by studies of other conformers besides the basic chairlike and boatlike conformers: tablelike [20], "zigzag" and "armchair" configurations [21], and a "stirrup" conformer [22]. Among these structural modes, the chairlike conformer has been employed most often when exploring the influence of the hydrogenation of graphene on its unique properties as a 2D crystal (as discussed in the "Introduction").

Despite the seemingly exhaustive exploration of the hydrogenated graphene structure, there are still issues that were not resolved by those studies. The first concerns the confirmation of the fluorine–hydrogen parallelism in regards to polyfluorides and polyhydrides of graphene. The second is related to the mechanism of the hydrogenation process, which evidently must proceed via the formation of the chairlike hexagonal cyclohexane pattern of graphane. The third is the question of the conditions under which the chairlike conformer can dominate over other conformers. To answer these questions, we must obtain a method of controlling the evolution of the hydrogenation of pristine graphene. The odd-electron molecular theory of sp^2 nanocarbons [55] is perfectly suited to this aim, as demonstrated by the computational design of polyderivatives of fullerene C_{60} under stepwise fluorination [56] and hydrogenation [57].

The computational design of sp^2 nanocarbon polyderivatives makes use of the peculiarities of the odd-electron

structure of fullerenes [58], nanotubes [36], and graphene [34, 55]. Due to exceeding C–C bond length the critical value $R_{CC}^{crit} = 1.395$ Å), under which a complete covalent bonding between odd electrons occurs only, thus transferring them into classical π electrons, the odd electrons become correlated and partially unpaired so that the species obtain a partially radical character [37, 55]. The unrestricted broken symmetry approach makes it possible to evaluate the total number of unpaired electrons in the structure (N_D), as well as its fraction on each atom (N_{DA}) that quantify the molecular chemical susceptibility (MCS) and the atomic chemical susceptibility (ACS), respectively [58]. Distributed over the molecule's atoms, the ACS forms a map of the chemical activity of the molecule, representing a "chemical portrait" of the molecule and indicating which sites have the highest chemical activities (high-rank ACS values). The site with the highest ACS value is the site that is targeted first in the chemical reaction. After this site has been attacked and the first derivative has been constructed, the ACS map of the latter highlights the target atom for the next chemical addition, meaning that the second derivative can be constructed, and so on. In other words, the reaction proceeds in an algorithmic (stepwise) manner, which forms the basis for the controlled computational design of polyderivatives, as guided by their ACS maps. This approach has been shown to be very effective for generating the polyfluoride and polyhydride families of C_{60}, as well as fullerene polycyanides and polyaziridines [59], polyamines with complicated structures [55], graphene-carbon nanotube composites [38], and fullerene C_{60}-based composites [39].

Using this algorithm, we have studied the stepwise computational synthesis of polyhydrides $(CH)_n$ through the serial addition of either hydrogen molecules or hydrogen atoms to a graphene molecule. A similar study concerning polyfluorides $(CF)_n$ is currently in progress. In our study, the graphene molecule was considered to be a membrane; the atoms of this membrane were accessible to adsorbate from either both sides or only one side of the membrane. The membrane was also either strictly fixed at its perimeter (a fixed membrane), or its edge atoms were allowed to move freely during the optimization procedure (a free-standing membrane). The main results, a detailed description of which will be published elsewhere, are as follows:

1. Molecular adsorption of hydrogen onto the graphene is weak, and adsorption onto both sides of a free-standing membrane is preferred in this case. This is accompanied by a small coupling energy and a low saturation coverage.
2. Atomic adsorption is strong, and the saturation coverage in this case is 100% or close to it. The adsorption pattern is a complicated mixture of different cyclohexane conformational motifs; the prevalence of each depends on whether the membrane is free-standing or fixed and on the accessibility of the membrane sides:
   a. Complete hydrogen coverage of a fixed membrane with both sides accessible results in a regular structure consisting of *trans*-coupled chairlike cyclohexane conformers, thus leading to chairlike graphane.
   b. Hydrogen adsorption onto a fixed membrane with one accessible side results in the continuous accommodation of tablelike cyclohexane conformers onto a convex surface, similar to a simple canopy.
   c. Hydrogen adsorption onto a free-standing membrane with the both sides accessible leads to a relatively extended graphane structure accompanied by the irregular packing of boatlike conformers.
   d. Hydrogen adsorption onto a free-standing membrane with one accessible side causes such a large degree of rolling of the pristine graphene sheet that conformer analysis of the final configuration is difficult.

The current paper focuses mainly on the formation of a regular graphane structure due to the adsorption of hydrogen atoms onto both sides of a fixed membrane; other adsorption modes are only considered briefly. The main topic can be attributed to real experimental conditions under which the appearance of graphane as a new 2D-crystal has been heralded [1]. The amorphous graphane obtained experimentally was attributed by the authors of [1] to one-sided adsorption on the ripples in graphene deposited on SiO_2 substrate. This case is similar to case (2b) of our study.

Calculations were performed in the framework of the unrestricted broken symmetry Hartree–Fock (UBS HF) scheme, implemented in the semiempirical AM1 version of the CLUSTER-Z1 code [60]. The algorithm for this is described in detail in [61].

The first stage of graphene hydrogenation

The graphene molecule selected for this study is a (5,5) rectangular nanographene according to the (n_a, n_z) classification suggested in [62]. n_a and n_z represent the number of benzenoid units along the armchair (*ach*) and zigzag (*zg*) edges of the graphene sheet, respectively. The equilibrium structure of the molecule along with its ACS map, which presents the distribution of atomically matched effectively unpaired electrons N_{DA} over the atoms in the graphene, are shown in Fig. 1. Panel (b) presents the ACS values at the positions of the atoms—the chemical portrait of the graphene sheet. Different ACS values are shown as different color intensities (see the attached scale). The absolute ACS

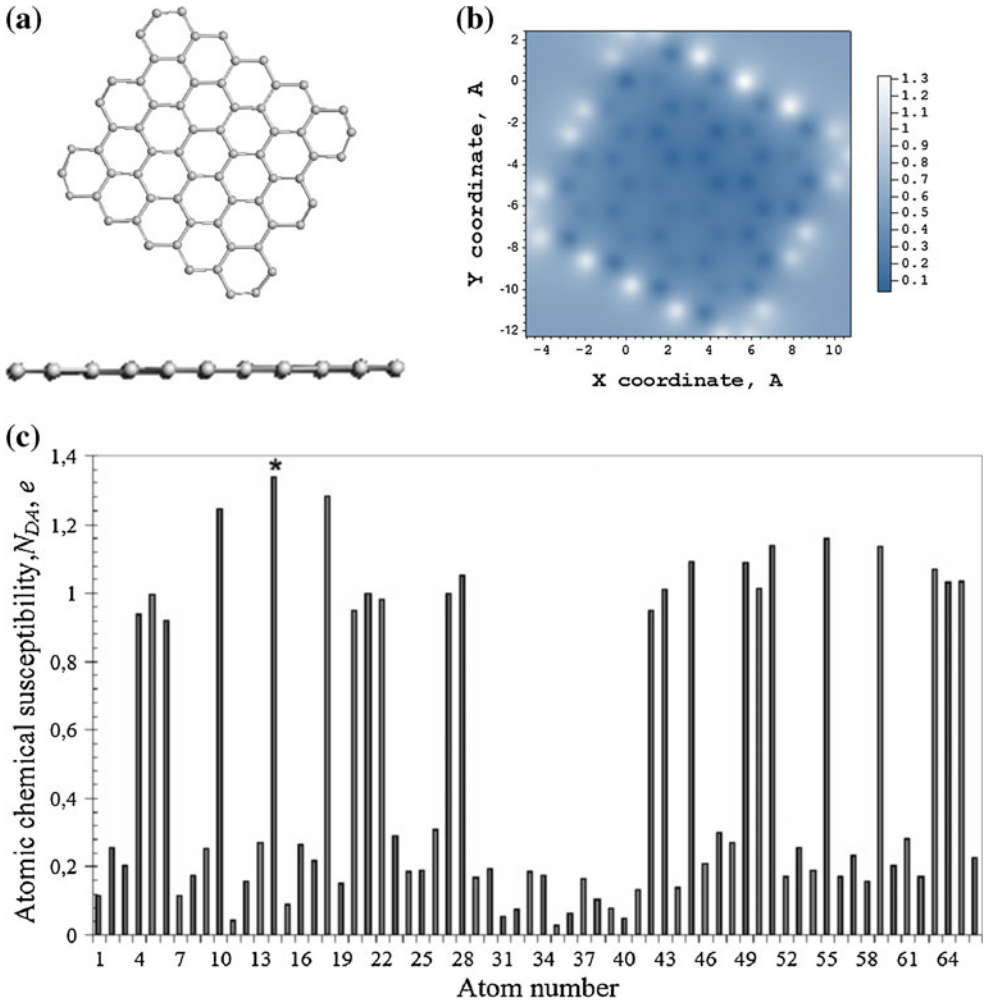

Fig. 1a–c Top and side views of the equilibrium structure of (5,5) nanographene (**a**), and the ACS distribution over its atoms in real space (**b**) and per atom (**c**; numbering is the same as that used in the output file)

values for different atoms (the numbering scheme corresponds to that used in the output file) are shown in panel (c). As seen in the figure, 22 edge atoms (2×5 *zg* and 2×6 *ach* ones) have the highest ACS, indicating that the perimeter is the most chemically active region of the molecule. The maximum ACS of 1.3 e and 1.1 e on the *zg* and *ach* atoms, respectively, demonstrate high radicalization of these atoms, and obviously suggest that the edge atoms provide the first targets for hydrogenation. It should be noted that the ACS values are directly connected with the spin density on the edge atoms (see detailed discussions of this topic in [33–37]), a subject that has been (and still is) actively discussed for about twenty years [19], since the first publication on it [63] in 1996. The appearance of the spin density highlights the spin contamination of the solution obtained for the singlet ground-state graphene (sheets, ribbons, molecules, quantum dots, etc.) when using single-determinant quantum schemes in either UBS DFT or UBS HF approaches. In the framework of these computational schemes, the spin density—should be zero for the singlet ground state—points directly to the correlation of odd electrons, which is followed by partial or complete unpairing of these weakly interacting electrons but not the magnetic susceptibility of the object (a recent comprehensive review of the theoretical aspects of this problem is given in [64]). The edge atoms are highlighted because each of them possesses two odd electrons, and the interaction between these electrons is obviously weaker than that seen for the basal atoms, so the degree of electron unpairing is also the highest for these atoms, and larger for *zg* edges than *ach* ones.

The hydrogenation of the (5,5) molecule begins on atom 14 (marked by an asterisk in Fig. 1c), as it has the highest ACS value in the output file. The next step in the reaction is also found to involve an atom at the edge, and this trend continues until each edge atoms has been saturated by a pair of hydrogen atoms, since the first 44 of these steps occur at edge atoms, based on the ACS scores for each step. The resulting "hydrogen-framed" graphene molecule is shown in Fig. 2, alongside with the corresponding ACS map. Two equilibrium structures are presented in this figure. The structure in panel (a) corresponds to the optimization of the molecule structure without any restrictions. When the positions of the edge carbon atoms and the framing hydrogen

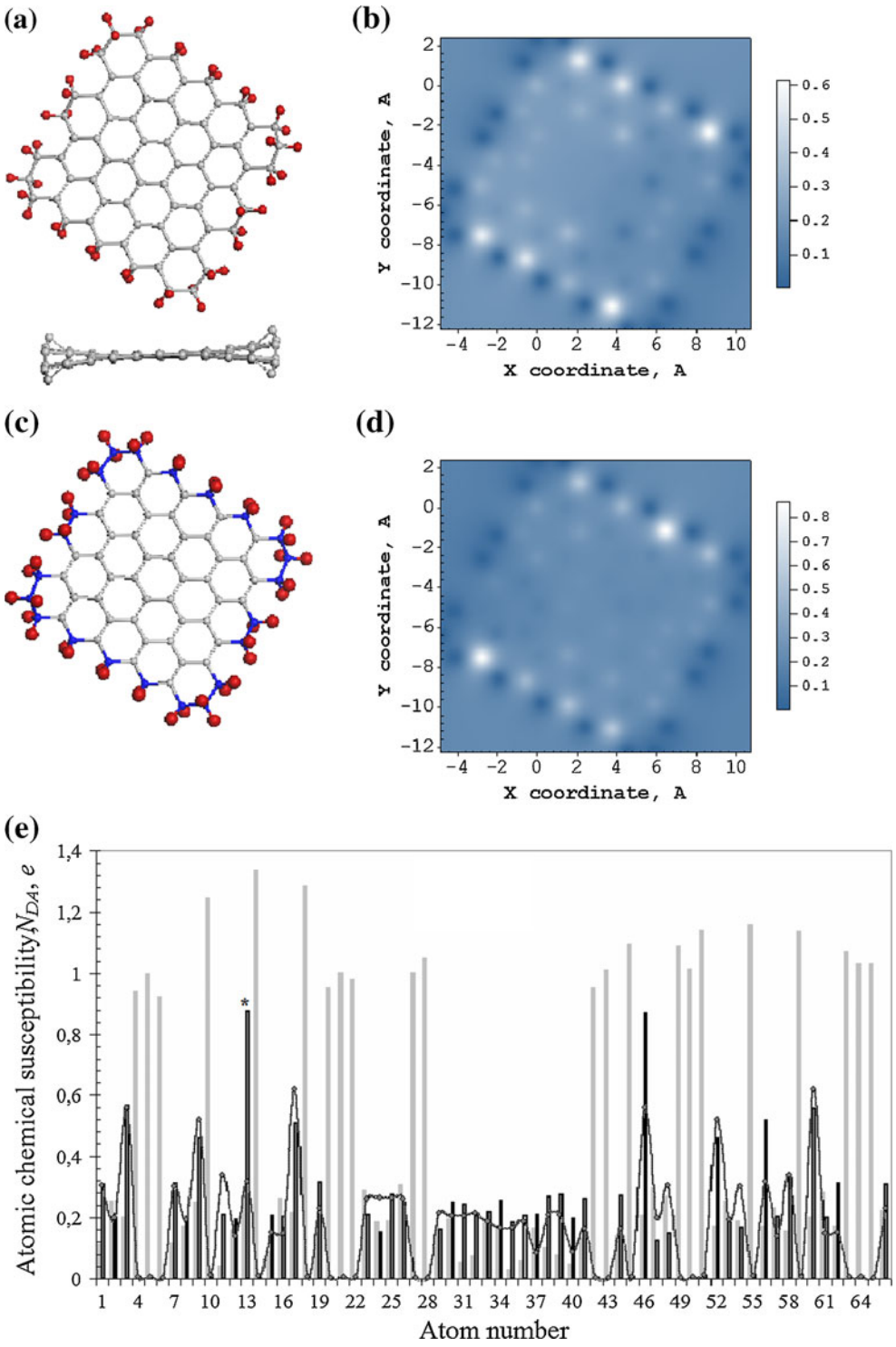

Fig. 2a–e Equilibrium structures of the free-standing (top and side views; **a**) and fixed (**c**) (5,5) nanographene membranes, and ACS distributions over their atoms in real space (**b**, **d**) and per atom (**e**; numbering scheme is the same as that used in the output file). The *light gray histogram* plots the ACS data for the pristine graphene. *Curve with dots* and *black histogram* relate to the membranes in panels **a** and **c**, respectively

atoms are fixed, optimization leads to the structure shown in panel (c). In what follows, we shall refer to these two structures as free-standing and fixed membranes, respectively. The blue carbon atoms in Fig. 2c, along with the framing hydrogens, are excluded from subsequent optimizations performed in the following hydrogenation steps.

The chemical portraits of the membranes shown in Fig. 2b and d are quite similar, and reveal the transformation of bright edge atoms in Fig. 1b into dark spots. The addition of two hydrogen atoms to each edge carbon saturates the valence of the latter completely, which results in zero ACS values, as is clearly seen in Fig. 2e. Chemical activity is then shifted to the neighboring inner atoms, and remains much more intense in the vicinity of the *zg* edge atoms. Since the ACS distribution synchronously reflects the distribution of C–C bonds with lengths of more than R_{crit}=1.395 Å in sp^2

structures [34, 35], the differences between Figs. 2b and d highlight the changes that occur to the C–C bond lengths in the free-standing membrane when its perimeter atoms are fixed.

Hydrogenation of the basal plane

The next stage of hydrogenation concerns the basal plane of the fixed membrane shown in Fig. 2c. To simplify the presentation of the subsequent results, the framing hydrogen atoms will not be shown in what follows. As seen in Fig. 2e, the first hydrogenation step should concern basal atom 13 (marked by an asterisk). According to our conditions, both sides of the membrane are accessible to hydrogen, so we have to check which side is more energetically favorable for hydrogen deposition: above the carbon plane ("up") or below it ("down"). As seen from Table 1, the up position is preferrable, and the equilibrium structure obtained, H1, is shown in Fig. 3. This structure is accompanied by the ACS map that makes it possible to trace the changes in the chemical activity of the graphene molecule during hydrogenation. Rows H*N* (*M*) in Table 1 display intermediate graphene hydrides involving *N* atoms of adsorbed hydrogen, where H0 is the pristine (5,5) molecule with 44 framing hydrogen atoms. *M* indicates the basal carbon atom to which the *N*th hydrogen atom is attached. Columns N_{DA} and N_{at} present the highest-rank ACS values and the numbers (i.e., from the atom numbering scheme) of the atoms to which they belong. The calculated heats of formation ΔH are subjected to the lowest-energy criterion for selecting the best isomorphs that are marked in Table 1 in italics.

After the deposition of hydrogen atom 1 onto basal atom 13, the ACS map reveals that carbon atom 46 is the target for the next deposition (see the ACS map for H1 in Fig. 3). The energy criterion convincingly favors the down position for hydrogen adsorption onto this atom, so we obtain structure H2 in Fig. 3. The deposition of the second hydrogen atom highlights the next target atom, 3 (see the ACS map of the H2 hydride), the adsorption of the third hydrogen atom indicates that the next target atom is 60, the fourth does the same for atom 17, and so forth. By checking the energies of the up and down depositions, it is possible to choose the best configuration of each hydride, and the corresponding equilibrium structures for a selected set of hydrides from H1 to H11 are shown in Fig. 3. Based on the results obtained, the first eight hydrogen atoms are deposited onto the substrate

Table 1 Intermediate steps in the hydrogenation of the (5,5) nanographene basal plane

N_{at}	N_{DA}	N_{at}	N_{DA}	N_{at}	N_{DA}	N_{at}	N_{DA}	N_{at}	N_{DA}	N_{at}	N_{DA}	N_{at}	N_{DA}	N_{at}	N_{DA}
H0		H1 (13)		H2 (46)		H3 (3)		H4 (60)		H5 (17)		H6 (52)		H7 (9)	
13	0.87475	*Up*		Up		*Up*		Up		*Up*		Up		*Up*	
46	0.87034	*46*	*0.62295*	3	0.56119	*60*	*0.55935*	17	0.54497	*52*	*0.49866*	56	0.47308	*56*	*0.47318*
3	0.56633	*3*	*0.61981*	60	0.55965	*17*	*0.54302*	56	0.50027	*56*	*0.47072*	9	0.47072	*12*	*0.42593*
60	0.55862	*60*	*0.56055*	17	0.54299	*56*	*0.51849*	52	0.49996	*9*	*0.36783*	12	0.36783	*8*	*0.42263*
56	0.51946	ΔH = *126.50*		ΔH = 101.88		ΔH = *96.88*		ΔH = 99.77		ΔH = *95.00*		ΔH = 96.82		ΔH = *97.50*	
17	0.50841	Down		*Down*		Down		*Down*		Down		*Down*		Down	
52	0.45883	46	0.62197	*3*	*0.56174*	60	0.55906	*17*	*0.54576*	52	0.49684	*9*	*0.47392*	56	0.46883
9	0.45843	3	0.62099	*60*	*0.55926*	17	0.54279	*56*	*0.49878*	56	0.49602	*56*	*0.47247*	12	0.41783
58	0.33071	60	0.55979	*17*	*0.54297*	56	0.51736	*52*	*0.49782*	9	0.47141	*12*	*0.36857*	8	0.41459
19	0.31539	ΔH = 127.54		ΔH = *98.19*		ΔH = 101.90		ΔH = *95.99*		ΔH = 99.40		ΔH = *96.23*		ΔH = 98.92	
H8 (56)		H9 (12)		H10 (57)		H11 (53)		H12 (58)		H13 (33)		H14 (30)		H15 (34)	
Up		Up		*Up*		*Up*		Up		*Up*		Up		Up	
12	0.42462	57	0.42824	*53*	*0.30873*	*58*	*0.54014*	33	0.33339	*30*	*0.40225*	34	0.34848	35	0.51203
8	0.42404	53	0.42131	*8*	*0.30851*	*30*	*0.32126*	8	0.30396	*34*	*0.3618*	31	0.33662	31	0.36904
53	0.41554	47	0.30877	*2*	*0.2956*	*8*	*0.32075*	2	0.29194	*8*	*0.34811*	8	0.2934	2	0.29541
ΔH = 99.83		ΔH = 118.04		ΔH = *79.46*		ΔH = *74.17*		ΔH = 73.81		ΔH = *65.87*		ΔH = 70.90		ΔH = 73.11	
Down		*Down*		Down		Down		*Down*		Down		*Down*		*Down*	
12	*0.4232*	*57*	*0.42759*	8	0.30801	58	0.58671	*33*	*0.32811*	30	0.40175	*34*	*0.34603*	*35*	*0.5002*
57	*0.42303*	*53*	*0.4216*	2	0.29368	8	0.32092	*8*	*0.30638*	34	0.3625	*31*	*0.3272*	*31*	*0.36752*
8	*0.42294*	*47*	*0.31082*	53	0.29305	30	0.30986	*2*	*0.28938*	8	0.34298	*2*	*0.29516*	*2*	*0.29455*
ΔH = *98.98*		ΔH = *89.19*		ΔH = 107.96		ΔH = 101.20		ΔH = *68.89*		ΔH = 84.89		ΔH = *67.58*		ΔH = *71.83*	

N_{at} number (from the atom labeling scheme) of the carbon atom, N_{DA} atomic chemical susceptibility, ΔH heat of formation of the hydride (kcal mol^{-1})

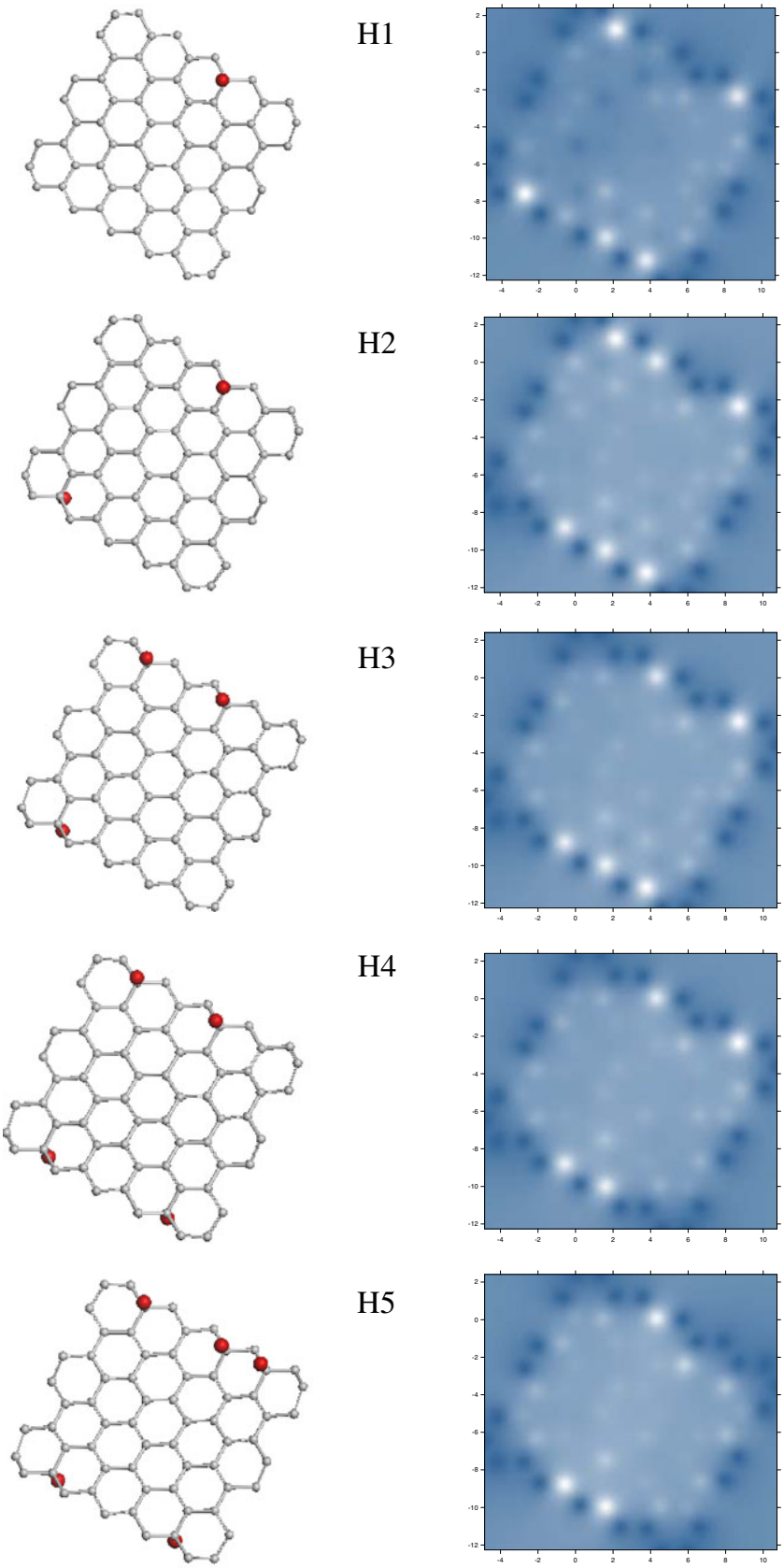

Fig. 3 Equilibrium structures (*left*) and real-space ACS maps (*right*) of intermediate hydrides produced during the initial stages of basal-plane hydrogenation

Fig. 3 (continued)

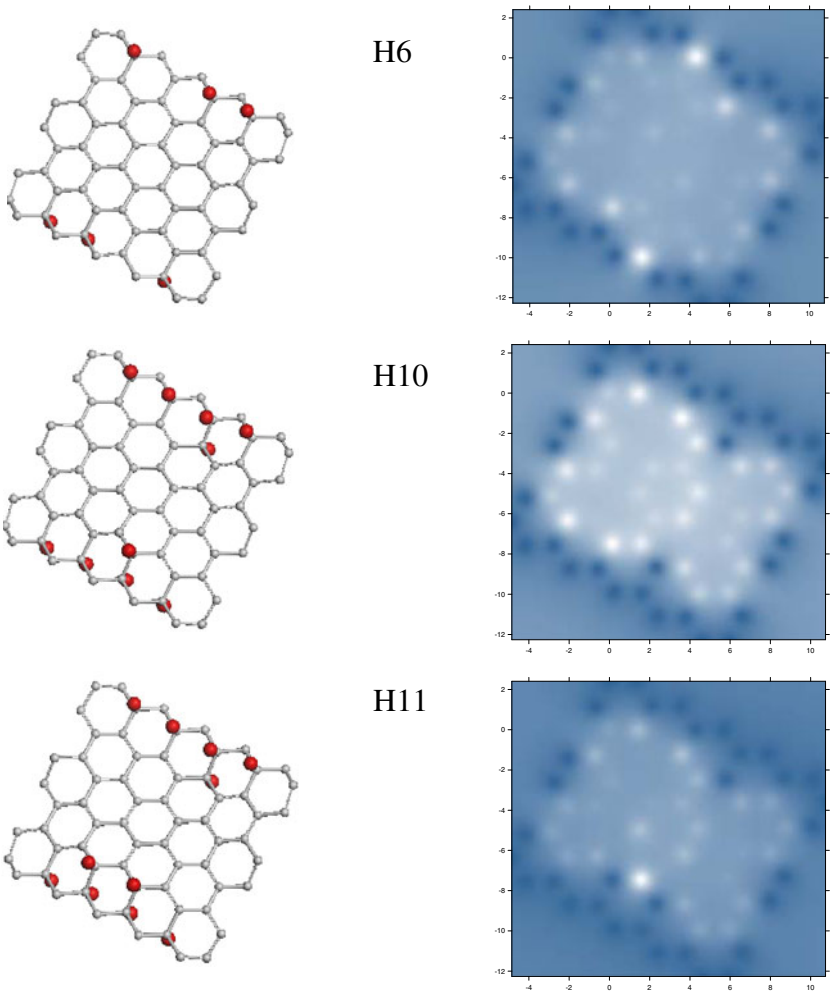

atoms characterized by the largest ACS peaks in Fig. 2b. After these highly active sites have been saturated, hydrogen adsorption starts to occur in the inner part of the basal space in a rather irregular manner, as can be seen in Figs. 3 and 4. The first hexagonal unit with the cyclohexane chairlike motif (cyclohexanoid chair) is formed when the number of hydrogen adsorbates reaches 38. This finding correlates well with experimental observations of a disordered, seemingly randomly distributed, arrangement of adsorbed hydrogen atoms on the graphene membrane at low coverage [65].

This computational scheme continues until the 34th step, when the ACS list contains only zero values, as shown in Table 2. The zero ACS values arise due to the continuous redistribution of excessively long C–C bonds across the graphene plane during hydrogenation. Leaving a detailed discussion of the changes in the nanographene structure caused by the $sp^2 \rightarrow sp^3$ transformations of the electronic configurations of the carbon atoms due to hydrogen adsorption to the next section, let us first draw attention to the considerable shortening of C–C bond lengths seen in Fig. 5 for H34 hydride. Five bonds 1.35 Å in length connect the remaining ten untouched basal sp^2carbon atoms. This C–C distance is much less than the critical C–C bond length, $R^{\mathrm{crit}}_{\mathrm{C-C}} = 1.395\,\text{Å}$, so the odd electrons of these atoms are covalently coupled in pairs (i.e., they are classical π electrons), with no effectively unpaired electrons. In this case, we can continue to consider the hydrogen adsorption individually for every pair, checking each atom of the pair for the preference of either up or down deposition. Thus (see Table 2), for the pair of connected atoms 19 and 16 that are highlighted by the ACS list in spite of the presence of zero quantities in the output file, the preference for the 35th down deposition should be given to atom 16. Attaching hydrogen to this atom immediately highlights its partner, atom 19, which becomes the target for the 36th up deposition. Considering the pair of joined atoms 54 and 29 discloses a preference for the up deposition on atom 29, and so forth, until the last atom (44) is occupied by adsorbate. The structure obtained at the end of the 44th step is shown at the bottom of Fig. 4. It is perfectly regular, including framing hydrogen atoms, and thus represents the computationally designed chairlike (5,5) nanographane.

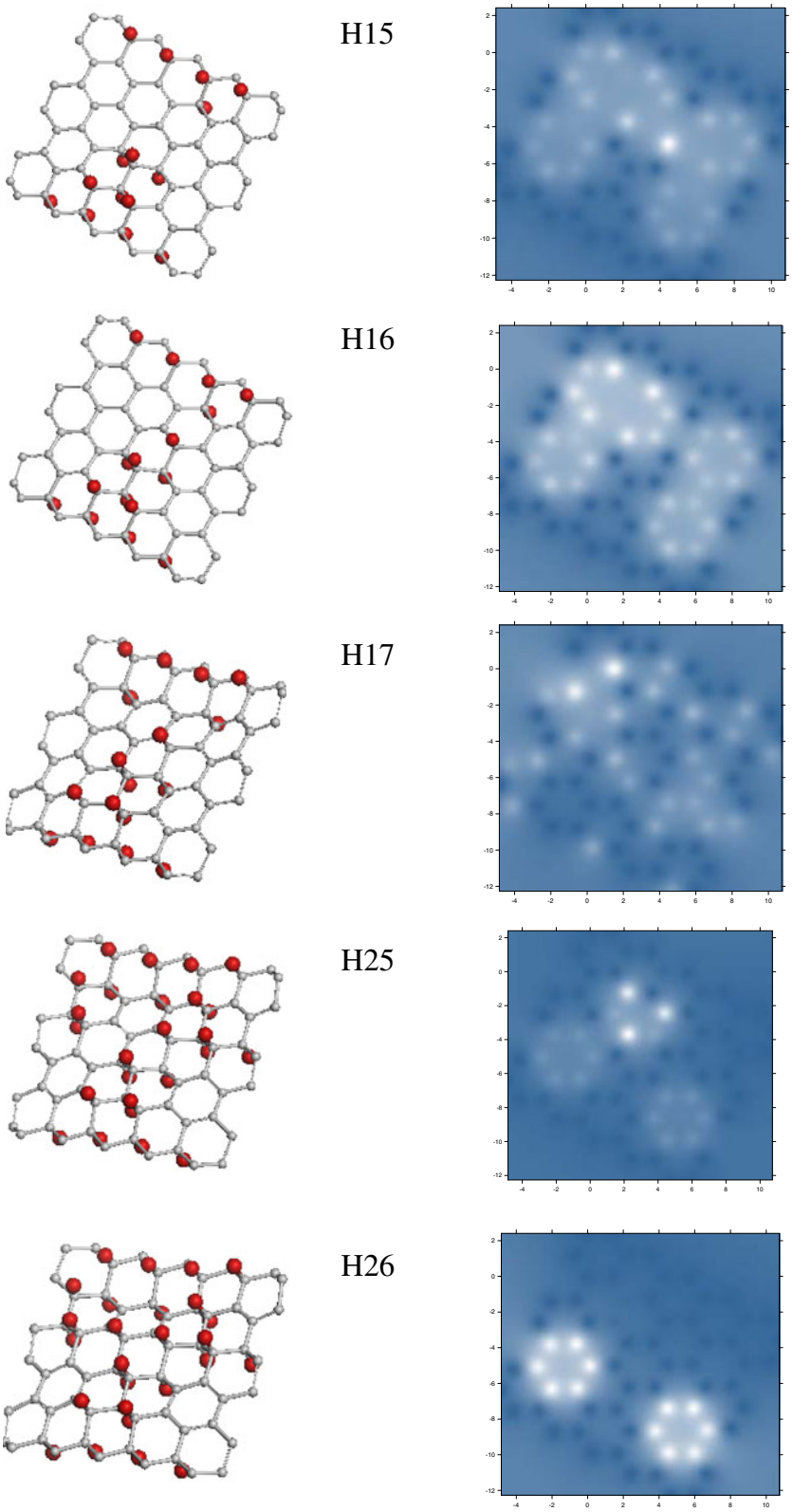

Fig. 4 Equilibrium structures (*left*) and real-space ACS maps (*right*) of hydrides produced during the concluding stages of basal-plane hydrogenation

Fig. 4 (continued)

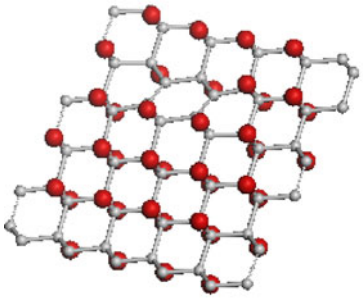

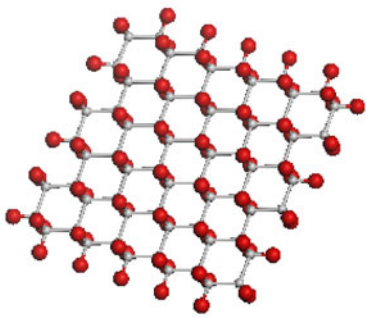

Hydrogenation-induced structural transformation of (5,5) nanographene

Stepwise hydrogenation is followed by the gradual substitution of the sp^2-configured carbon atoms of the pristine graphene molecule by the sp^3 atoms of graphane. Since the valence angles between the corresponding C–C bonds and the bond lengths are noticeably different in the two cases, the structure of the pristine nanographene becomes markedly distorted. The formation of the chair-like hexagonal pattern is another reason for the serious violation of the pristine near-planar structure. The necessary modifications to the basal plane structure are clearly apparent in Fig. 4.

Figure 5 demonstrates the transformation of the molecule's structure during the hydrogenation process, exemplified by the changes that occur to a fixed set of C–C bonds. The light gray curve shifted up by 0.15 Å in each panel presents the reference bond length distribution for the pristine nanographene framed by 44 hydrogen atoms that saturate all "dangling bonds" of the edge atoms of the graphene. As seen in the figure, the first hydrogenation steps are

Table 2 Final steps in the hydrogenation of (5,5) nanographene basal plane

N_{at}	N_{DA}	N_{at}	N_{DA}	N_{at}	N_{DA}	N_{at}	N_{DA}	N_{at}	N_{DA}	N_{at}	N_{DA}
H33 (66)		H34 (41)		H35 (16)		H36 (19)		H37 (29)		H38 (54)	
Up		*Up*		Up		*Up*		*Up*		Up	
41	0.87719	*19*	*0.00011*	19	0.87268	*54*	*0*	*54*	*0.88406*	37	0
143	0.03036	*16*	*0.00011*	145	0.03623	*29*	*0*	*147*	*0.02945*	62	0
137	0.02556	*115*	*0*	134	0.02774	*7*	*0*	*121*	*0.02916*	120	0
ΔH = 17.51		$\Delta H = -20.25$		ΔH = 1.45		$\Delta H = -52$		$\Delta H = -118.95$		ΔH = −115.63	
Down		Down		*Down*		Down		Down		*Down*	
41	*0.87536*	19	0	*19*	*0.88234*	54	0	54	0.8823	*37*	*0*
85	*0.03146*	16	0	*107*	*0.0311*	29	0	147	0.03469	*62*	*0*
137	*0.03045*	115	0	*134*	*0.02987*	7	0	121	0.02329	*137*	*0*
$\Delta H = 6.36$		ΔH = 19.00		$\Delta H = -27.22$		ΔH = −19.03		ΔH = −105.70		$\Delta H = -147.29$	
H39 (37)		H40 (62)		H41 (32)		H42 (7)		H43 (36)		H44 (11)	
Up		Up		Up		*Up*		Up		*Up*	
62	*0.88414*	7	0	7	0.88308	*11*	*0*	11	0.88222	*53*	*0*
149	*0.02943*	32	0	151	0.03496	*36*	*0*	153	0.0351	*1*	*0*
120	*0.02886*	11	0	135	0.02033	*126*	*0*	119	0.02231	*128*	*0*
$\Delta H = -147.15$		ΔH = −144.19		ΔH = −162.81		$\Delta H = -201.06$		ΔH = −187.39		$\Delta H = -227.61$	
Down		*Down*		*Down*		Down		*Down*		Down	
62	0.88269	*7*	*0*	*7*	*0.88315*	11	0	*11*	*0.88403*	48	0
149	0.0346	*32*	*0*	*151*	*0.03071*	36	0	*153*	*0.02955*	20	0
120	0.02261	*11*	*0*	*127*	*0.02866*	136	0	*119*	*0.02884*	23	0
ΔH = −134.71		$\Delta H = -175.29$		$\Delta H = -173.52$		ΔH = −170.64		$\Delta H = -200.10$		ΔH = −198.25	

N_{at} number (from the atom labeling scheme) of the carbon atom, N_{DA} atomic chemical susceptibility, ΔH heat of formation of the hydride (kcal mol^{-1})

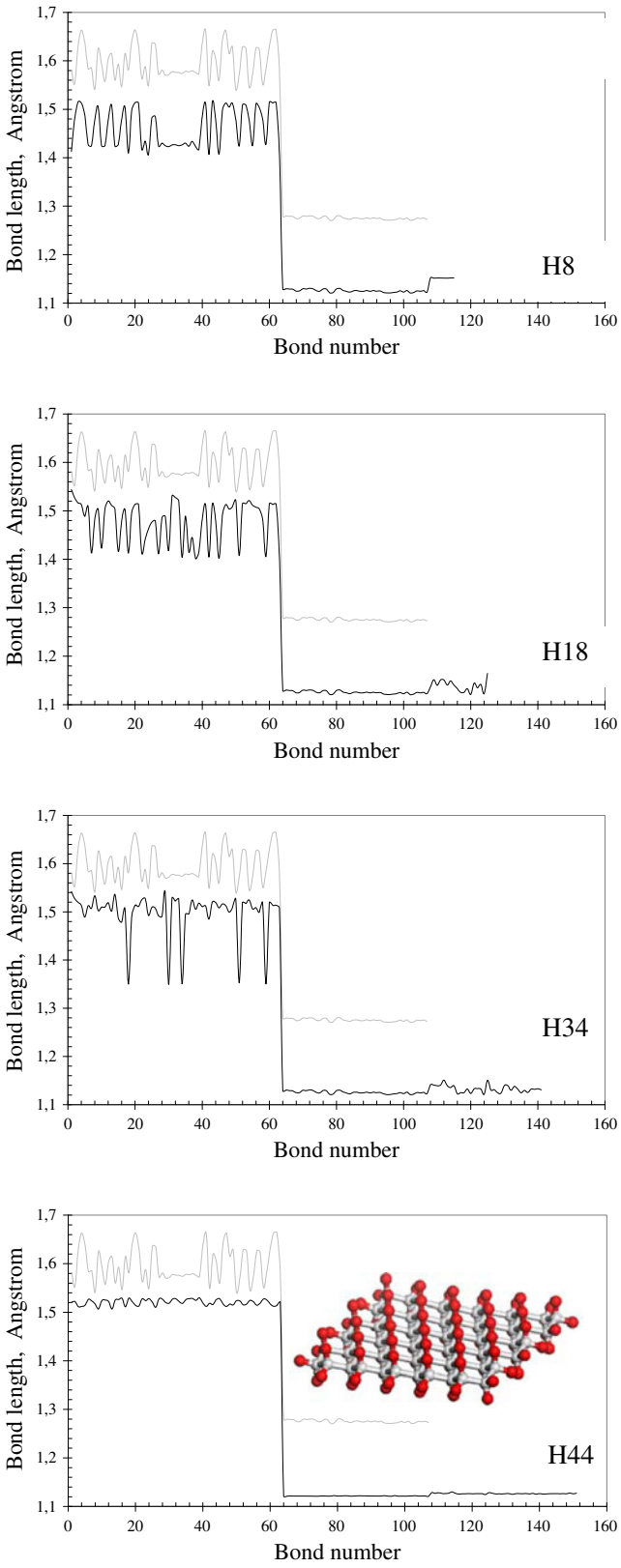

Fig. 5a–d $sp^2 \rightarrow sp^3$ transformation of the graphene structure during serial hydrogenation. *Gray* and *black curves* correspond to the distributions of the length of C–C and C–H bonds in the hydrogen-framed pristine graphene and its hydrides, respectively

followed by the elongation of C–C bonds that involve not only the newly formed sp^3-hybridized atoms but also some of the sp^2-hybridized ones too.

Comparing the diagram for the pristine graphene with those for the current hydrogenated species makes it possible to trace the changes in molecular structure. As might naturally be expected, the $sp^2 \rightarrow sp^3$ transformation causes the appearance of elongated C–C bonds, and the number of these elongated bonds increases as hydrogenation proceeds. To keep the carbon skeleton closed and to minimize the deformation caused by the structural distortion, some C–C bonds shorten in length, as already mentioned. However, when hydrogenation is complete, a perfectly regular structure is obtained, in contrast to the rather irregular structure of the pristine framed nanographene.

The behavior of the hydrogen atoms added can be characterized by the average length of the C–H bonds that they form. As seen in Fig. 5, 44 newly formed bonds in the hydrogen-framed pristine graphene are quite uniform, with an average value of 1.126 Å. This value slightly exceeds the accepted C–H length for hydrocarbons of 1.10–1.11 Å. This does not indicate inconsistency in the computational program, as the UBS HF calculations within the AM1 version provide a C–H bond length of 1.10 Å for many other hydrocarbons, including the aromatic family from benzene to penthacene, as well as for H-terminated carbon nanotubes. However, the same computational scheme provides longer C–H bonds of 1.127 Å for fullerene hydrides [57] and H-terminated graphene, whether monoatom-terminated [33–35] or diatom-terminated. In the latter case, the matter is about peripheral framing conserving empty basal plane. As soon as the hydrogenation starts to proceed in the basal plane, the length of the C–H bonds rapidly increase—they are 1.152 Å for H8, 1.139 Å for H18, and 1.133 Å for H34 (see Fig. 5)—but they decrease back to the average length of the framing C–H bonds (1.122 Å) when the regular graphane structure is completed. A similar situation is observed in the case of fullerene C_{60} hydrides: incomplete hydrogenation is followed by elongated C–H bonds (1.146 Å on average), but the bond lengths equilibrate to 1.127 Å upon the completion of hydrogenation [57].

Energetic characteristics accompanying (5,5) nanographene hydrogenation

The total coupling energy, which characterizes the hydrogenation of the molecule, can be calculated using

$$E_{\mathrm{cpl}}^{\mathrm{tot}}(n) = \Delta H_{n\mathrm{Hgr}} - \Delta H_{\mathrm{gr}} - n\Delta H_{\mathrm{at}} \quad (1)$$

Here $\Delta H_{n\mathrm{Hgr}}$, ΔH_{gr}, and ΔH_{at} are the heats of formation of a graphene hydride with n hydrogen atoms, the pristine

nanographene, and the hydrogen atom, respectively. This energy is found to be negative, with an absolute value that gradually increases as the number of attached hydrogen atoms grows. This finding indicates that the stepwise hydrogenation of (5,5) nanographene considered in this study is energetically profitable.

The tempo of hydrogenation can be characterized by the coupling energy needed for the addition of a hydrogen atom at each step. This can be determined via

$$E_{\mathrm{cpl}}^{\mathrm{step}}(n) = \Delta H_{n\mathrm{Hgr}} - \Delta H_{(n-1)\mathrm{Hgr}} - \Delta H_{\mathrm{at}} \quad (2)$$

Evidently, both the total and per-step coupling energies, as well as the total energy of the hydride $\Delta H_{n\mathrm{Hgr}}$, are due to both the deformation of the graphene molecule's carbon skeleton and the covalent coupling of hydrogen atoms to its atoms during the formation of C–H bonds. Assuming that the relevant contributions can be summed, we can try to evaluate them separately. Thus, the total deformation energy can be determined as the difference

$$E_{\mathrm{def}}^{\mathrm{tot}}(n) = \Delta H_{n\mathrm{Hgr}}^{\mathrm{sk}} - \Delta H_{\mathrm{gr}}. \quad (3)$$

Here, $\Delta H_{n\mathrm{Hgr}}^{\mathrm{sk}}$ is the heat of formation of the carbon skeleton of the studied hydride at the nth hydrogenation step. This value can be obtained through one-point-structure determination of the equilibrium hydride after removing all of the hydrogen atoms. The deformation energy that accompanies each step of the hydrogenation can be determined as follows:

$$E_{\mathrm{def}}^{\mathrm{step}}(n) = \Delta H_{n\mathrm{Hgr}}^{\mathrm{sk}} - \Delta H_{(n-1)\mathrm{Hgr}}^{\mathrm{sk}}, \quad (4)$$

where $\Delta H_{n\mathrm{Hgr}}^{\mathrm{sk}}$ and $\Delta H_{(n-1)\mathrm{Hgr}}^{\mathrm{sk}}$ are the heats of formation of the carbon skeletons of the relevant hydrides at two subsequent hydrogenation steps. Similarly, the total and per-step chemical contributions caused by the formation of C–H bonds can be determined as

$$E_{\mathrm{cov}}^{\mathrm{tot}}(n) = E_{\mathrm{cpl}}^{\mathrm{tot}}(n) - E_{\mathrm{def}}^{\mathrm{tot}}(n) \quad (5)$$

and

$$E_{\mathrm{cov}}^{\mathrm{step}}(n) = E_{\mathrm{cpl}}^{\mathrm{step}}(n) - E_{\mathrm{def}}^{\mathrm{step}}(n-1). \quad (6)$$

Figure 6 displays the energies calculated for a complete set of hydrides formed through the stepwise hydrogenation of a (5,5) nanographene fixed membrane. The zero points on the horizontal axes correspond to the membrane that is framed by 44 hydrogen atoms but has an empty basal plane. As seen in Fig. 6a, the total hydride energy $\Delta H_{n\mathrm{Hgr}}$ is actually the difference between two big numbers, and the absolute values of both of them increase as the number of hydrogen atoms added grows. The difference remains positive—although it gradually decreases—up to the 32th step, indicating that the deformational energy dominates over the total energy during those hydrogenation steps. At the 32th step, $\Delta H_{n\mathrm{Hgr}}$changes sign, showing that the chemical contribution becomes dominant. The per-step energies in Fig. 6c clearly demonstrate that hydrogenation is an energetically profitable reaction until it is completed, when all basal carbon atoms are involved in the process. The detailed behavior of the deformation energy and the chemical contribution can be used to explore each hydrogenation step in depth.

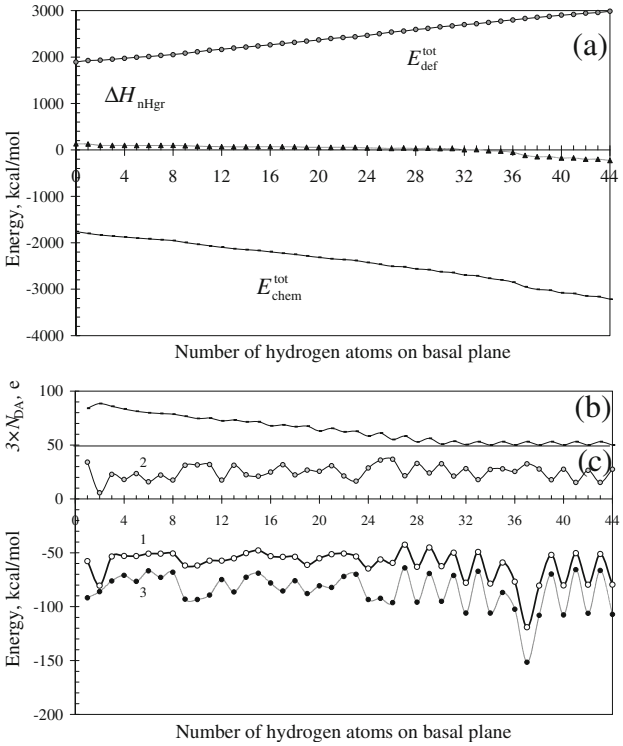

Fig. 6a–c Energetic and electronic characteristics of the graphene hydrides. **a** Total energy $\Delta H_{(n-44)\mathrm{Hgr}}$; $E_{\mathrm{def}}^{\mathrm{tot}}(n-44)$ and $E_{\mathrm{cov}}^{\mathrm{tot}}(n-44)$ (see Eqs. 3 and 5). **b** Total number of effectively unpaired electrons. **c** Per-step energies $E_{\mathrm{cpl}}^{\mathrm{step}}(n-44)$ (*1*); $E_{\mathrm{def}}^{\mathrm{step}}(n-44)$ (*2*); $E_{\mathrm{cov}}^{\mathrm{step}}(n-44)$(*3*)

The efficacy of the chemical reactions involved in the formation of polyderivatives of sp^2 nanocarbons can be characterized by the behavior of the total number of effectively unpaired electrons, N_{D}, in the molecule during the reaction [56]. The initial N_{D} value for the (5,5) nanographene molecule studied is 31.04 e. After framing the edge atoms with 44 hydrogens, this value decreases to 13.76 e, and the gradual dissipation of this pool of chemical susceptibility during the course of basal plane hydrogenation is presented in Fig. 6b. To better show the N_{D} data using the scale employed in Fig. 6c, these data have been multiplied by 3 and shifted up by 50 units. As seen in Fig. 6b, hydrogenation is accompanied by a gradual decrease in the value of N_{D} until it reaches zero at the 32th step. The subsequent hydrogenation steps were discussed in the previous section. Generally, the hydrogenation of (5,5) nanographene proceeds in a very similar manner to that of fullerene C_{60} [57].

Discussion and concluding remarks

The transformation of a graphene molecule into graphane, as considered above, is not the only consequence of the adsorption of hydrogen onto a graphene sheet (in other words, its chemical modification through hydrogenation). During our investigations, including but not limited to those presented above, we have found that both the hydrogenation itself and the final hydrides formed depend on several external factors, namely: whether the graphene substrate is fixed; the accessibility of the sides of the substrate to the hydrogen; and whether the hydrogen vapor is molecular or atomic. These factors mean that, whether performing a computational study or exploring the technology of graphene hydrogenation, it is necessary to consider a significant number of modes at the same time—always at least eight, provided that molecular and atomic adsorption do not occur simultaneously. Detailed consideration of all the alternative modes should be mandatory for any serious project aimed at using graphene-based nanomaterials in, say, hydrogen-stored fuel cells [66]. We have performed only the first few steps along this path, by exploring all of the hydrogenation modes related to atomic adsorption onto (5,5) nanographene; two molecular adsorption modes were considered. In all cases, the attachment of the hydrogen atoms to the carbon atoms of the substrate was realized by the algorithm described in "Algorithmic computational design of graphene polyhydrides $(CH)_n$." In spite of the limitations caused by considering only one substrate model, the conclusions obtained allow us to suggest a relatively complete picture of the events that accompany the hydrogenation of graphene, as summarized in Table 3. Based on these results, we will now try to answer the questions we posed earlier:

1. Is the adsorption of molecular hydrogen or that of atomic hydrogen more probable?

As follows from Table 3, our study has convincingly shown that only atomic adsorption is effective and energetically favorable, which is consistent with the widely known fact that molecular hydrogen adsorption onto graphite is extremely rare. This conclusion is additionally supported by the fact that all of the studies were performed using the same substrate: the basal plane of (5,5) nanographene with 44 framing hydrogen atoms.

Figure 7 presents equilibrium structures of the final hydrides obtained during the adsorption of molecular hydrogen onto the basal plane (accessible to the hydrogen from both sides) of free-standing (a) and fixed (b) membranes. The choice of the target atoms for the molecule deposition followed the ACS algorithm described earlier. The coupling energy of the products is determined as

$$E_{cpl}^{tot}(n) = \Delta H_{nH_2gr} - \Delta H_{gr} - n\Delta H_{H_2}. \quad (7)$$

Here, ΔH_{nH_2gr}, ΔH_{gr}, and ΔH_{H_2} are the heats of formation of a graphene hydride with n hydrogen molecules, the pristine graphene, and the hydrogen molecule ($\Delta H_{H_2} = -5.182$ kcal mol^{-1}), respectively. As seen in the figure, the adsorption of the first hydrogen molecule is accompanied by the formation of two C–H bonds 1.18 Å in length. The second molecule is not adsorbed when it approaches the substrate, whichever side it approaches from. However, keeping the molecule in the vicinity of the graphene substrate significantly lowers its energy. The addition of the third molecule prompts the adsorption of the second one, while the third molecule is not adsorbed. As in the previous case, the formation of this complex leads to a gain in energy. The fourth molecule is then willingly adsorbed, while the fifth all the way up to the fifteenth molecule is not. Therefore, molecular hydrogen adsorption leads to a basal plane hydrogen coverage of about 14%.

In the case of a fixed membrane (Fig. 7b), the adsorption of the first hydrogen molecule requires 11.7 kcal mol^{-1}. In contrast to the free-standing membrane, none of the subsequent hydrogen molecules are adsorbed, thus providing very low (4.5%) coverage of the basal plane. At the same time, keeping the molecules in the vicinity of the substrate increases the energy.

Table 3 Final products of the adsorption of hydrogen onto (5,5) nanographene

Atomic or molecular hydrogen adsorption onto nanographene?	Fixed or free-standing membrane?	Access of hydrogen to membrane	
		Access to both sides of membrane	Access to one side of membrane
Atomic adsorption	Fixed membrane	Hydride of regular graphane structure (100% hydrogen coverage); see Fig. 8a	Hydride of a canopy structure (96% hydrogen coverage); Fig. 8b
	Free-standing membrane	Hydride of regular graphane structure accompanied by fragments of amorphous structure (100% hydrogen coverage); see Fig. 9a	Hydride of a basket structure (100% hydrogen coverage); see text and Fig. 9b
Molecular adsorption	Fixed membrane	Hydride of nonplanar sheet structure (~5% hydrogen coverage); see Fig. 7b	No results
	Free-standing membrane	Hydride of an irregular bent sheet structure (10–15% hydrogen coverage); see Fig. 7a	No results

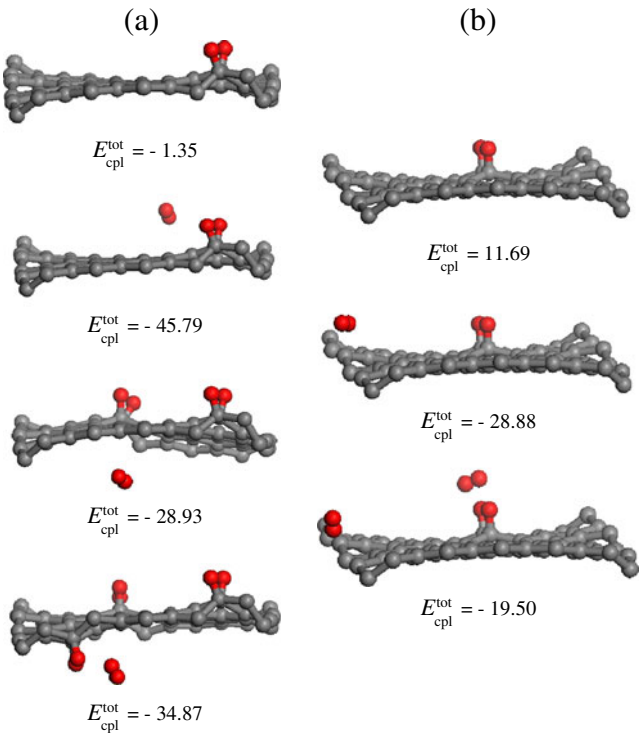

Fig. 7a–b Equilibrium structures of hydrides formed during the molecular adsorption of hydrogen onto free-standing (**a**) and fixed (**b**) (5,5) nanographene membranes, which are accessible to the adsorbate from both sides of the membrane. E^{tot}_{cpl} is the total coupling energy (see Eq. 7). The framing hydrogen atoms are not shown

For atomic hydrogen adsorption, the formation of hydrides with practically complete coverage of the basal plane turns out to be quite possible. Figure 8 presents the final hydrides formed during atomic hydrogen adsorption onto the basal plane of a fixed membrane. When both sides of the membrane are accessible to hydrogen atoms, the complete hydrogenation of the graphene corresponds to the formation of a graphane

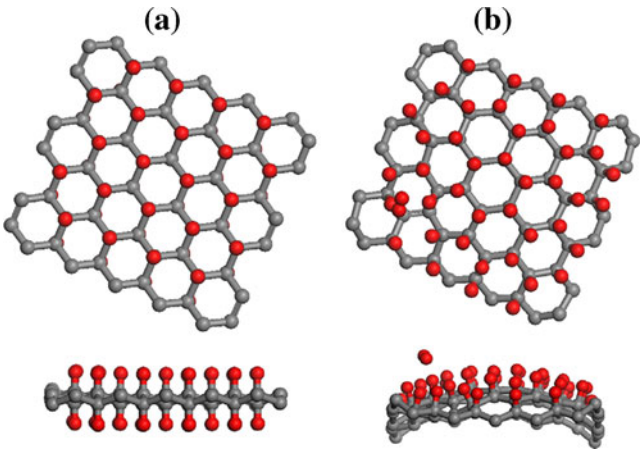

Fig. 8a–b Two views of the equilibrium structures of hydrides formed during the adsorption of atomic hydrogen onto a fixed (5,5) nanographene membrane that is accessible to the adsorbate from both sides (**a**) or just one side (**b**)

regular structure with 100% hydrogen coverage (Fig. 8a), as described in the preceding sections. If the membrane is accessible from only one side, serial attachment of hydrogen atoms to the substrate causes its carbon skeleton to arch, ultimately resulting in a canopy shape (Fig. 8b). During the formation of this canopy, the C–C bonds lengthen to 1.51–1.53 Å. However, when the membrane edges are fixed, not all bonds are able to meet the requirements of this structure, so some of them remain quite short. In this case, a pair of hydrogen atoms that need to attach to two carbon atoms (forming bonds) are not allowed to attach, thus prompting the atoms to associate and form a hydrogen molecule outside of the basal plane. In the current study, the last atoms 43 and 44 exhibited this behavior, resulting in the desorption of one hydrogen molecule and lowering the plane coverage to 96%.

At first glance, the final stage of the adsorption of hydrogen atoms onto a free-standing membrane accessible from both sides (Fig. 9a) appears to be similar to that presented in Fig. 8a. However, a closer look reveals that the chairlike configuration of cyclohexanoids that occurs towards the top of the membrane is disrupted at the bottom of the membrane; in other words, the membrane contains a mixture of conformers that causes the regular structure of the carbon skeleton to distort. While this distortion does not prevent 100% hydrogen coverage of the basal plane from being achieved, the membrane becomes a mixture of a region containing the regular graphane structure and some regions containing amorphous structure. Obviously, the relative contribution of each component depends on the size of the graphene sample.

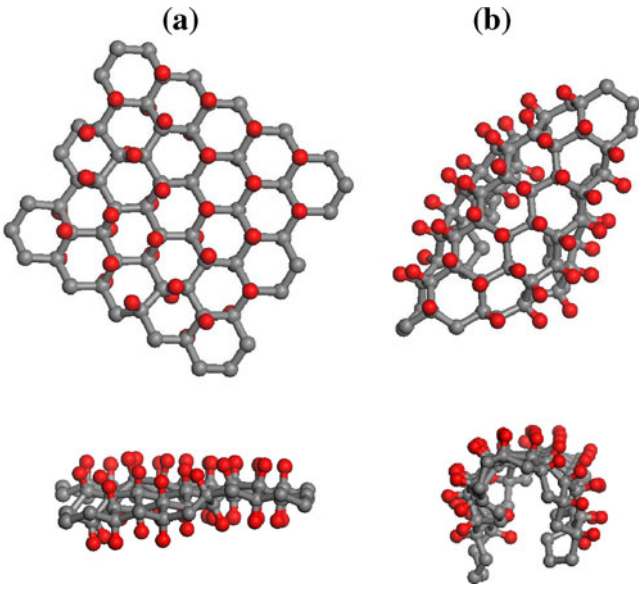

Fig. 9a–b Two views of the equilibrium structures of hydrides formed during the adsorption of atomic hydrogen onto a free-standing (5,5) nanographene membrane that is accessible to the adsorbate from both sides (**a**) or just one side (**b**)

In contrast to the discussion above, the adsorption of hydrogen via just one side of the free-standing membrane results in the formation of a peculiar basket shape (this shape occurs when two diagonally opposite corners of a rectangular figure are brought close together; see Fig. 9b). The formation of this strangely shaped hydride with 100% hydrogen coverage is accompanied by an energy gain of ~1 kcal mol^{-1} per carbon atom.

We might suppose that the reason for this dramatic difference between atomic and molecular hydrogen adsorption is the tendency of the graphene substrate to conserve the hexagonal pattern. Clearly, this pattern can only be conserved if the hydrogenation of the substrate results in the creation of a cyclohexane-patterned structure based on one of the conformers of this structure, or a mixture of such conformers. If the uncoordinated deposition of individual atoms (as we saw in Figs. 3 and 4) can meet this requirement, the coordinated deposition of two atoms onto neighboring carbons of the substrate obviously makes the formation of a cyclohexane-conformer pattern much less probable.

2. What is the characteristic image of the attachment of hydrogen atoms to the substrate?

The hydrogen atom is deposited onto the carbon in both the up and down configurations. In contrast to a vast number of organic molecules, the lengths of the C–H bonds formed during adsorption exceed 1.1 Å, varying for different adsorption events. The lengths of the C–H bonds are quite constant (1.122 Å on average) for the framing hydrogens that saturate the edge carbon atoms of the substrate. Deposition onto the basal plane causes the bond lengths to increase up to maximum of 1.152 Å. However, the formation of a regular chairlike-cyclohexane structure like graphane leads to bond equilibration, and the bonds decrease to 1.126 Å in length. This scenario, which is characteristic of a fixed membrane that is accessible from both sides, is significantly violated when considering a fixed membrane that is only accessible from one side, or a free-standing membrane that is accessible from both sides; the strength of bonding between the hydrogen atoms and the substrate in the latter two cases is significantly different from that seen for a fixed membrane that is accessible from both sides.

3. Which carbon atom(s) is/are the first target(s) for hydrogen attachment?

4. How are carbon atoms selected for subsequent adsorption steps?

Using an approach already successfully applied to fullerenes and carbon nanotubes [55], the formation of graphene polyhydride $(CH)_n$ is considered above in the framework of algorithmic stepwise computational design, in which each subsequent step is controlled by the distribution of the atomic chemical susceptibility in terms of fractional numbers of effectively unpaired electrons on atom, N_{DA}, of the preceding derivative over the substrate atoms. Ranking the N_{DA} values definitely distinguishes the atoms that serve as targets for subsequent chemical attack. Additionally, the lowest-energy criterion indicates the most energetically stable hydride. The successful generation of fluoride and hydride polyderivatives—as well as other polyderivatives of fullerene C_{60} [55]; the polyhydride $(CH)_n$ with 100% hydrogen coverage, related to chairlike graphane (described in the current paper); as well as the tablelike-cyclohexane hydride $(CH)_n$ with a canopy shape and 96% hydrogen coverage—demonstrates the high efficacy of this approach for monitoring the process of polyderivative formation, which makes it possible to gain deep insight into the mechanism of these chemical transformations.

5. Is there any connection between the sequential adsorption pattern and the formation of cyclohexane conformers during hydrogenation?

The investigations performed here have shown that there is a direct connection between the state of the graphene substrate and the conformer pattern of the polyhydride obtained. The pattern is governed by which of the cyclohexane conformers is most profitably (from an energy perspective) formed under ambient conditions. Thus, a regular chairlike-cyclohexane-conformed graphene with 100% hydrogen coverage (i.e., graphane) is formed when the graphene substrate is a fixed-perimeter membrane that can be accessed by the hydrogen adsorbate on both sides. When both sides of the membrane are accessible but its edges are not fixed, the formation of a mixture of chairlike- and boatlike-cyclohexane patterns is found to be the most profitable. The difference in the behavior of the two membranes is caused by so-called *H frustration* [48], which refers to a configuration where a sequence of alternating up and down H atoms is broken (frustrated). H frustration increases out-of-plane distortions, which induces in-plane dimensional shrinkage. Additionally, as shown in the current paper, the total energy of the polyhydride involves deformational and chemical components. That is why, even though it is more energetically favorable to form the chairlike conformer rather than the boatlike conformer in the free-standing membrane per se, the formation of the boatlike conformer also leads to a significant gain in energy due to the deformation of the carbon skeleton, which compensates for the difference in energy between the two conformers. The formation of the boatlike conformer leads to significant corrugation of the initial graphene plane, and the presence of a mixture of the two conformers transforms the regular crystalline behavior of graphane into partially amorphous-like behavior in the latter case.

When the fixed membrane is only accessible from one side, the configuration produced is relatively regular, and looks like an infinite array of *trans*-linked tablelike-cyclohexane conformers. The coupling of hydrogen atoms with the carbon skeleton is characterized by long C–H bonds 1.18–1.21 Å in length. The carbon skeleton adopts the shape of a canopy. Hydrogenation of this kind can occur under particular energetically rich conditions, such as hydrothermal conditions. This finding sheds light on the genesis of the mineraloid shungite (Sheka EF, Rozhkova NP, Popova NA, 2011, private communication), which consists of globules of compressed, concave, saucer-like graphene sheets, and forms in the Earth's core under the influence of high temperature and pressure as well as a high concentration of hydrogen atoms.

Acknowledgments The authors greatly appreciate fruitful discussions with K. Novoselov.

References

1. Elias DC, Nair RR, Mohiuddin TMG, Morozov SV, Blake P, Halsall MP, Ferrari AC, Boukhvalov DW, Katsnelson MI, Geim AK, Novoselov KS (2009) Science 323:610–613
2. Romanchemko V (2009) 3D News: Daily Digital Digest http://www.3dnews.ru/editorial/it-graphane
3. Dresselhaus MS, Araujo PT (2010) ACS Nano 4:6297–6302
4. Chakraborty T (2010) Phys Can 66:289–291
5. Quintana M, Spyrou K, Grzelczak M, Browne WR, Rudolf P, Prato M (2010) ACS Nano 4:3527–3533
6. Balog R, Jørgensen B, Nilsson L, Andersen M, Rienks E, Bianchi M, Fanetti M, Lægsgaard E, Baraldi A, Lizzit S, Sljivancanin Z, Besenbacher F, Hammer B, Pedersen TG, Hofmann P, Hornekær L (2010) Nat Mater 9:315–319
7. Lee J-H, Grossman JC (2010) Appl Phys Lett 97:133102
8. Zhou J, Wang Q, Sun Q, Chen XS, Kawazoe Y, Jena P (2009) Nano Lett 9:3867–3870
9. Savini G, Ferrari AC, Giustino F (2010) Phys Rev Lett 105:037002
10. Cudazzo P, Attaccalite C, Tokatly IV, Rubio A (2010) Phys Rev Lett 104:226804
11. Crassee I, Levallois J, Walter AL, Ostler M, Bostwick A, Rotenberg E, Seyller T, van der Marel D, Kuzmenko AB (2011) Nat Phys 7:48–51
12. Singh AK, Penev ES, Yakobson BI (2010) ACS Nano 4:3510–3514
13. Muñoz E, Singh AK, Ribas MA, Penev ES, Yakobson BI (2010) Diam Rel Mat 19:368–373
14. Topsakal M, Cahangirov S, Ciraci S (2010) Appl Phys Lett 96:091912
15. Pei QX, Zhang YW, Shenoy VB (2010) Carbon 48:898–904
16. Openov LA, Podlivaev AI (2010) JETP Lett 90:459–463
17. Openov LA, Podlivaev AI (2010) Tech Phys Lett 36:31–33
18. Schmidt MJ, Loss D (2010) Phys Rev B 82:085422
19. Culchac FJ, Latgé A, Costa AT (2011) New J Phys 13:033028
20. AlZahrania AZ, Srivastava GP (2010) Appl Surf Sci 256:5783–5788
21. Leenaerts O, Peelaers H, Hernandez-Nieves AD, Partoens B, Peeters FM (2010) Phys Rev B 82:195436
22. Bhattacharya A, Bhattacharya S, Majumder C, Das GP (2011) Phys Rev B 83:033404
23. Sahin H, Ataca C, Ciraci S (2010) Phys Rev B 81:205417
24. Ju W, Wang H, Li T, Fu ZH, Zhang Q (2010) Key Eng Mater 434–435:803–804
25. Cheng SH, Zou K, Okino F, Gutierres HR, Gupta A, Shen N, Eklund PC, Sofo JO, Zhu J (2010) Phys Rev B 81:205435
26. Nair RR, Ren WC, Jalil R, Riaz I, Kravets VG, Britnell L, Blake P, Schedin F, Mayorov AS, Yuan S, Katsnelson MI, Cheng HM, Strupinski W, Bulusheva LG, Okotrub AV, Grigorieva LV, Grigorenko AN, Novoselov KS, Geim AK (2010) Small 6:2877–2884
27. Zboril R, Karlicky F, Bourlinos AB, Steriotis TA, Stubos AK, Georgakilas V, Safárová K, Jancík D, Trapalis C, Otyepka M (2010) Small 6:2885–2891
28. Rosas JJH, Gutiérrez RER, Escobedo-Morales A, Chigo Anota E (2011) J Mol Model 17:1133–1139
29. Loh KP, Bao Q, Ang PK, Yang J (2010) J Mat Chem 20:2277–2289
30. van den Brink J (2010) Nat Mater 9:91–292
31. Abergel DSL, Apalkov V, Berashevich J, Ziegler K, Chakraborty T (2010) Adv Phys 59:261–282
32. Allouche A, Jelea A, Marinelli F, Ferro Y (2006) Phys Scr T124:91–95
33. Sheka EF, Chernozatonskii LA (2010) Int J Quantum Chem 110:1466–1480
34. Sheka EF, Chernozatonskii LA (2010) J Exp Theor Phys 110:121–132
35. Sheka EF, Chernozatonskii LA (2010) Int J Quantum Chem 110:1938–1946
36. Sheka EF, Chernozatonskii LA (2009) Nanostruct Mat Phys Model 1:115–149
37. Sheka EF (2012) arXiv 1201.5388v1 [condmat. mtrl-sci] Computational strategy for graphene: insight from odd electrons correlation
38. Sheka EF, Chernozatonskii LA (2010) J Theor Comput Nanosci 7:1814–1824
39. Sheka EF, Shaymardanova LKH (2011) J Mat Chem 21:17128–17146
40. Sheka EF, Popova NA, Popova VA, Nikitina EA, Shaymardanova LKH (2011) J Mol Model 17:1121–1131
41. Sheka EF, Popova NA, Popova VA, Nikitina EA, Shaymardanova LKH (2011) J Exp Theor Phys 112:602–611
42. Sheka EF, Popova NA (2011) J Phys Chem C 115:23745–23754
43. Jeloaica L, Sidis V (1999) Chem Phys Lett 300:157–163
44. Sha X, Jackson B (2002) Surf Sci 496:318–330
45. Hornekær L, Sljivancanin ZS, Xu W, Otero R, Rauls E, Stensgaard I, Lægsgaard E, Hammer B, Besenbacher F (2006) Phys Rev Lett 96:156104
46. Ito A, Nakamure H, Takayama A (2008) J Phys Soc Jpn 77:114602
47. Casolo S, Lovvik OM, Martinazzo R, Tantardini GF (2009) J Chem Phys 130:054704
48. Flores MZS, Autreto PAS, Legoas SB, Galvao S (2009) Nanotechnology 20:465704
49. Rüdorff W (1959) Adv Inorg Chem 1:223–266
50. Charlier J-C, Gonze X, Michenaud J-P (1993) Phys Rev B 47:16162–16168
51. Ebbert LB, Brauman JI, Huggins RA (1974) J Am Chem Soc 96:7841–7842
52. Boltalina OV, Bühl M, Khong A, Saunders M, Street JM, Taylor R (1999) J Chem Soc Perkin Trans 2:1475–1479
53. Taylor R (2004) J Fluor Chem 125:359–368
54. Sofo JO, Chaudhari AS, Barber GD (2007) Phys Rev B 75:153401
55. Sheka EF (2011) Fullerene nanoscience: nanochemistry, nanomedicine, nanophotonics, nanomagnetism. CRC, Boca Raton
56. Sheka EF (2010) J Exp Theor Phys 111:395–412
57. Sheka EF (2011) J Mol Model 17:1973–1984
58. Sheka EF (2007) Int J Quantum Chem 107:2803–2816
59. Sheka EF (2011) J Mol Model. doi:10.1007/s00894-011-1158-5

60. Zayets VA (1990) CLUSTER-Z1: quantum-chemical software for calculations in the *s*,*p*-basis. Institute of Surface Chemistry, National Academy of Sciences, Kiev
61. Berzigiyarov PK, Zayets VA, Ginzburg IY, Razumov VF, Sheka EF (2002) Int J Quantum Chem 88:449–464
62. Gao X, Zhou Z, Zhao Y, Nagase S, Zhang SB, Chen Z (2008) J Phys Chem A 112:12677–12682
63. Nakada K, Fujita M, Dresselhaus G, Dresselhaus MS (1996) Phys Rev B 54:17954–17961
64. Lain L, Torre A, Alcoba DR, Bochicchio RC (2011) Theor Chem Acc 128:405–410
65. Meyer JC, Girit CO, Crommie MF, Zettl A (2008) Nature 454:319–322
66. Nechaev YS (2011) Open Fuel Cells J 4:16–29